Available online at www.sciencedirect.com
ScienceDirect
Journal of the European Ceramic Society 28 (2008) 2771–2776
www.elsevier.com/locate/jeurceramsoc

The synthesis and polymorphic phase transitions of $Ba_4Nb_2O_9$ ceramics

Jana Bezjak [a,*], Boštjan Jančar [a], Aleksander Rečnik [b], Danilo Suvorov [a]

[a] *Advanced Materials Department, Jožef Stefan Institute, Jamova cesta 39, SI-1000 Ljubljana, Slovenia*
[b] *Nanostructured Materials Department, Jožef Stefan Institute, Jamova cesta 39, SI-1000 Ljubljana, Slovenia*

Received 16 December 2007; received in revised form 3 April 2008; accepted 4 April 2008
Available online 13 June 2008

Abstract

Perovskite-based ceramics within the BaO–$(Nb, Ta)_2O_5$ system possess excellent microwave dielectric properties, which make them suitable for applications in communication systems. The polymorphic phase transitions and the stability of the individual polymorphs of tetra-barium di-niobate (V) ($Ba_4Nb_2O_9$) were studied at different temperatures $Ba_4Nb_2O_9$ ceramics were prepared via a conventional solid-state reaction route. Three $Ba_4Nb_2O_9$ polymorphs were isolated. These include a hexagonal (α) and two orthorhombic (γ, β) modifications. Transmission electron microscopy (TEM) revealed an intergranular BaO-rich amorphous phase and nano-crystalline $Ba_5Nb_4O_{15}$ in all the polymorphs, most abundantly in the α-modification. Superstructure ordering in the α-modification was confirmed by electron diffraction methods. The α-$Ba_4Nb_2O_9$ was observed to be stable in the temperature range 560–1160 °C; below 560 °C the stable polymorph is β-$Ba_4Nb_2O_9$, while above 1160 °C the only stable polymorph is γ-$Ba_4Nb_2O_9$.

Keywords: Powders-solid-state reaction; Phase relations; Grain boundaries; X-ray methods; Niobates]

1. Introduction

Recent investigations have revealed that ceramics based on hexagonal perovskites exhibit attractive microwave dielectric properties with moderate quality factors ($Qxf > 30{,}000$ GHz) and dielectric constants ($\varepsilon_r > 30$) as well as a low-temperature dependence of resonant frequency ($-50 < \tau_f < +50$ ppm/K). [1–12] In contrast to the archetypical cubic perovskites, the crystal structure of the hexagonal perovskites comprise face-sharing BX_6 octahedra along close-packed AX_3 layers comprising the (1 1 1) planes of the perovskite lattice. The layers of face-sharing octahedra break the usual *ccp* stacking along the <1 1 1> axes, the structure locally acquires the *hcp* stacking, and the axis normal to this layer becomes the *c*-axis of the hexagonal structure [13]. When layers of face-sharing octahedra appear at regular intervals along the crystallographic *c*-axis this results in polytypic structures with hexagonal (H) and rhombohedral (R) symmetries.

In the BaO–Nb_2O_5–WO_3 and BaO–Ta_2O_5–WO_3 ternary systems Kemmler-Sack et al.[14–20] reported on a series of hexagonal perovskites. Vineis et al.[2] demonstrated that an 8-layer hexagonal perovskite, $Ba_8ZnTa_6O_{24}$, forms as a consequence of ZnO volatilization from the cubic perovskite $Ba_3ZnTa_2O_9$,[21] which is widely utilized for the production of high-Q base-station resonators in wireless telecommunications networks.[22] Furthermore, Mallinson et al.[9] identified the new, 10-layer hexagonal perovskites $Ba_{10}Mg_{0.25}Ta_{7.9}O_{30}$ and $Ba_{10}Co_{0.25}Ta_{7.9}O_{30}$. It is also known that $Ba_5Nb_4O_{15}$ and $Ba_5Ta_4O_{15}$ are B-site cation-deficient hexagonal perovskites with a *hhccc* stacking of BaO_3 layers .[23–25] The literature data suggest that the BaO-rich parts of the BaO–Ta_2O_5 and BaO–Nb_2O_5 systems should be prone to the formation of hexagonal perovskite phases.

Because of the potentially interesting microwave dielectric materials, we focused on the BaO-rich region of the BaO–Nb_2O_5 binary system,[26–29] where various hexagonal perovskite polytypes have been reported.[30–33] Even though the BaO–Nb_2O_5 binary system was extensively studied by several authors, the literature on many compounds in the BaO-rich part of this binary system, in particular of the $Ba_4Nb_2O_9$ polymorphs, is scarce and contradictive.[29–34] Furthermore, the crystal structures of the $Ba_4Nb_2O_9$ modifications have not yet been solved. Based on X-ray diffraction data Leshchenko et al. reported four different polymorphs of $Ba_4Nb_2O_9$, i.e., α, β, β′ and γ.[31–32] The α-modification was obtained by quenching the sample from 750 °C in an atmosphere of air, the β-modification was

* Corresponding author. Tel.: +386 1 4773 547; fax: +386 1 4773 221.
E-mail address: jana.bezjak@ijs.si (J. Bezjak).

0955-2219/$ – see front matter © 2008 Elsevier Ltd. All rights reserved.
doi:10.1016/j.jeurceramsoc.2008.04.003

formed by slow cooling from 1400 °C, and the γ-modification was obtained by quenching the sample from 1500 °C.[31] The α-$Ba_4Nb_2O_9$ also forms during slow cooling from about 1130 °C, while quenching the sample from above 1130 °C results in the formation of the γ-modification. Upon annealing at between 260 and 320 °C the γ-modification converts into the β-modification, which subsequently converts to the β′-modification when heated in a temperature range between 530 and 700 °C, and undergoes an irreversible phase transition into the α-modification at 700–1130 °C.[32]

Due to inconsistencies regarding the phase transitions and the stability of the $Ba_4Nb_2O_9$ modifications, we have reinvestigated the formation conditions of the individual polymorphs. To further understand the polymorphic transitions in this compound we sintered $Ba_4Nb_2O_9$ at different temperatures and in various atmospheres to verify the stability of the individual polymorphs. The samples were characterized using X-ray powder diffraction (XRD) and differential thermal analysis (DTA) whereas the presence of secondary phases and possible super-structural ordering were studied using transmission electron microscopy (TEM) techniques.

2. Experimental

The starting materials employed were high-purity powders of $BaCO_3$ (99.8%, Alfa Aesar) and Nb_2O_5 (99.8%, Alfa Aesar). The corresponding mixture was first ball-milled for 2 h (200 min^{-1}) with yttria-stabilized zirconia balls using ethanol as a mixing media. After drying the powder was calcinated at 800 °C in air for 20 h, then ground, and recalcined at 900 and 1000 °C for 20 h in order to ensure a complete reaction between the $BaCO_3$ and the Nb_2O_5. The powders were then uniaxially pressed into 10 mm pellets, under a pressure of 2 kN. The green bodies were sintered on a sacrificial pellet of the same composition in an alumina crucible at 1100, 1200 and 1300 °C in ambient air. The selected temperatures ensured sub-solidus conditions and did not exceed the decomposition temperatures of compounds.

After the calcinations and sintering the phase composition of each sample was analyzed by X-ray powder diffraction using a PAnalytical X'Pert PRO MPD high-resolution X-ray diffractometer with Cu Kα1 radiation (1.5406 Å) operated at 45 kV and 40 mA.

The homogeneity of the samples was studied with a scanning electron microscope (SEM; Jeol JSM-5800, Jeol Ltd., Tokyo, Japan) operated at 20 kV and equipped with a back-scattered electron (BEI) detector and an energy-dispersive X-ray spectrometer (EDS; Link ISIS 300, Oxford Instruments, Oxford, UK). In order to verify the presence of secondary phases at the grain boundaries we used a transmission electron microscope (TEM; JEM-2100, Jeol Ltd., Tokyo, Japan) operated at 200 kV. For the TEM observations the samples were cut into 3 mm discs, which were mechanically thinned and polished to a thickness of ~100 μm and dimpled (Dimple Grinder, Gatan Inc., Warrendale, PA) to ~20 μm in the disk center. The TEM specimens were produced by ion-milling (RES 010, Bal-Tec AG, Balzers, Liechtenstein) with 4 keV Ar^+ ions at an incidence angle of 10° until perforation of the central disk area.

3. Results and discussion

3.1. α-$Ba_4Nb_2O_9$ modification

The X-ray diffraction analysis of the powder mixture with a molar ratio $BaO:Nb_2O_5 = 4:1$ after firing at different temperatures between 800 and 1100 °C (Fig. 1) for 20 h indicates that the first binary phase, which forms below 800 °C, is a 5-layer (5L) hexagonal perovskite $Ba_5Nb_4O_{15}$. Additional peaks in the XRD spectra, accompanied by a decrease of the $BaCO_3$ and $Ba_5Nb_4O_{15}$ peaks, appear after firing at 900 °C. These peaks could be assigned to the α-$Ba_4Nb_2O_9$ modification described by Leshchenko et al., (ICDD file #35-1154).[31] By increasing the firing temperature to 1000 °C the diffraction peaks of the $BaCO_3$ disappear, whereas the peaks of $Ba_5Nb_4O_{15}$ disappear after firing at 1100 °C.

Furthermore, the X-ray diffraction patterns shown in Fig. 1 reveal the presence of broad peaks with low intensity, which appear after firing above 900 °C. Similar XRD patterns were also observed after firing at 1200 and 1300 °C. These diffraction peaks could either be a consequence of the presence of a secondary phase or a type of super-structural ordering in the $Ba_4Nb_2O_9$ phase. The SEM/EDS analysis of the ceramics prepared from α-$Ba_4Nb_2O_9$ powder sintered at 1100 °C in air showed no evidence for the presence of any secondary phases. As the unidentified reflections in the XRD pattern are weak and broad, this could indicate that secondary phases, if at all present, are nano-crystalline. In order to identify possible secondary phases at the grain boundaries in this sample we used a TEM (Fig. 2a). Even with moderate magnifications we were able to observe an abundant amorphous inter-granular phase

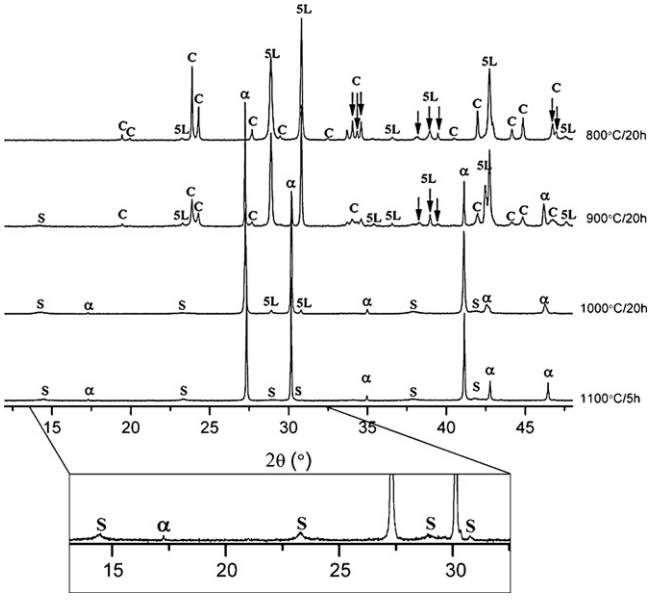

Fig. 1. X-ray powder-diffraction data for $Ba_4Nb_2O_9$ over the temperature range $800 < T < 1100$ °C (α indicates α-$Ba_4Nb_2O_9$ phase, 5L indicates $Ba_5Nb_4O_{15}$ phase, C indicates $BaCO_3$ and S indicates unidentified weak and broad peaks).

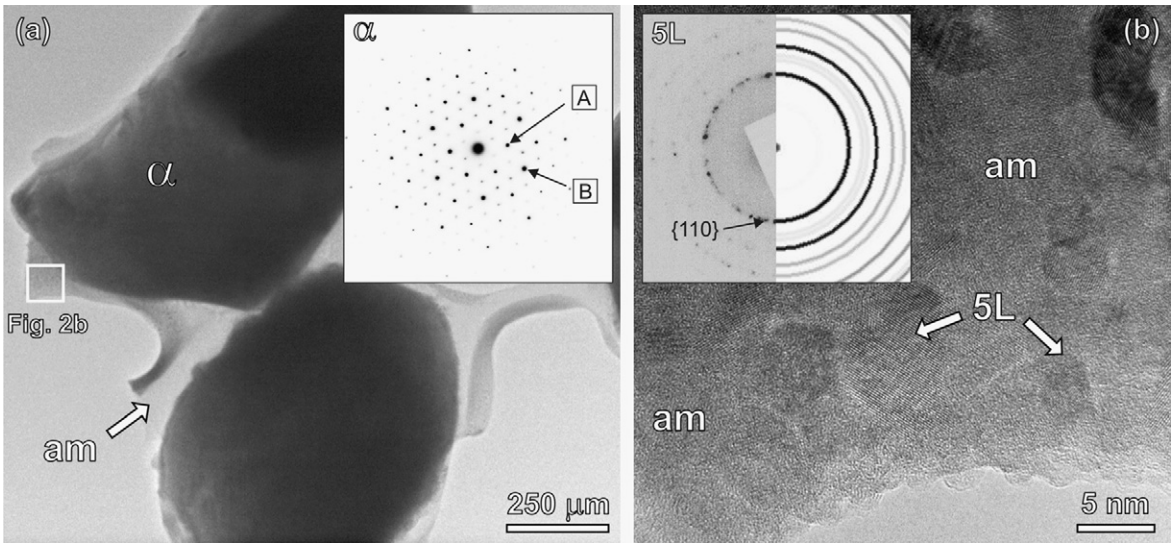

Fig. 2. (a) A bright-field TEM micrograph of α-$Ba_4Nb_2O_9$ shows matrix-phase grains (α) and an inter-granular amorphous phase (am). The inset in the upper-right corner shows a SAED pattern collected from α-$Ba_4Nb_2O_9$ grains. The diffraction spot A corresponds to $(1\,0\,0)_L = (2\,2\,0)_T$, and the spot B corresponds to $(1\,1\,0)_L = (6\,0\,0)_T$ (the subscripts L and T refer to indexing according to Leshchenko et al.[31] and Trunov et al.,[27] respectively). The square on the left-hand side of the micrograph shows the area enlarged in Fig. b. (b) A HRTEM micrograph shows the presence of nano-sized $Ba_5Nb_4O_{15}$ crystals (5L) within the amorphous phase. The inset shows a SAED pattern collected from nano-crystals and the simulated pattern corresponding to $Ba_5Nb_4O_{15}$ crystals.

between individual $Ba_4Nb_2O_9$ grains. At higher magnifications we found that this inter-granular phase is not homogeneous, but contains scattered 2–5 nm large nano-crystals (Fig. 2b). The selected area electron diffraction (SAED) patterns of these nano-crystals (inset in Fig. 2b) correspond to the $Ba_5Nb_4O_{15}$ phase. This is further confirmed by the EDS analysis of the nano-crystals, which shows a decrease in the Ba/Nb ratio with respect to the well-crystallized $Ba_4Nb_2O_9$ grains. On the other hand, the composition of the amorphous phase indicates a higher Ba/Nb ratio than that found for the $Ba_4Nb_2O_9$ grains. The presence of a BaO-rich amorphous phase and the nano-crystals of $Ba_5Nb_4O_{15}$ suggest the decomposition of α-$Ba_4Nb_2O_9$.

These observations, however, do not explain the weak, broad reflections in the XRD spectra. The SAED patterns of the matrix-phase grains (inset in Fig. 2a) indicate their hexagonal symmetry and the main diffraction spots can be indexed either to the reduced hexagonal-cell of the α-$Ba_4Nb_2O_9$ modification, as proposed by Leshchenko et al.,[31] or to the hexagonal super-structure (ICDD file #46-0939), as reported by Trunov et al.[27] Based on a analogy with the $Ba_4Ta_2O_9$ structure,[35] Leshchenko et al.[31] described some reflections as super-structural. For this reason the unit-cell constants ($a = 5.923$ Å and $c = 4.230$ Å) were interpreted as sub-structural, while the super-structural peaks evident from the XRD pattern were not considered in the calculation of the unit-cell dimensions. In the analysis of the XRD data by Trunov et al.[27] most of the weak reflections were included and indexed as a hexagonal super-structural cell ($a = 20.52$ Å and $c = 8.452$ Å), which also corresponds to our electron diffraction data. If our SAED pattern is indexed according to the unit-cell proposed by Leshchenko et al.[31] the diffraction spot A (see the inset of Fig. 2a) would be indexed as (1 0 0), whereas according to Trunov et al.[27] this spot is indexed as (2 2 0), indicating that their unit-cell is rotated by 30°, with respect to the sub-cell of Leshchenko et al.,[31] and multiplied along the *a*-axis. Similarly, the reflection spot B from our SAED pattern, can be indexed using the unit-cell of Leshchenko et al.[31] as (1 1 0), and according to Trunov et al.[27] as (6 0 0). The super-structural reflections in our SAED pattern (see the inner ring of weak reflections in the inset of Fig. 2a) and most of the remaining weak reflections in our XRD pattern suggest that the structure of α-$Ba_4Nb_2O_9$ indeed has a hexagonal symmetry with unit-cell parameters that correspond to those proposed by Trunov et al.[27]

3.2. γ-$Ba_4Nb_2O_9$ modification

When α-$Ba_4Nb_2O_9$ is heated above 1200 °C and quenched to room temperature the recorded XRD pattern corresponds to the γ-modification of $Ba_4Nb_2O_9$ (ICDD file #35-1156).[31] The XRD spectra of the samples sintered at 1200 and 1300 °C for 5 h and quenched to room temperature are shown in Fig. 3. In

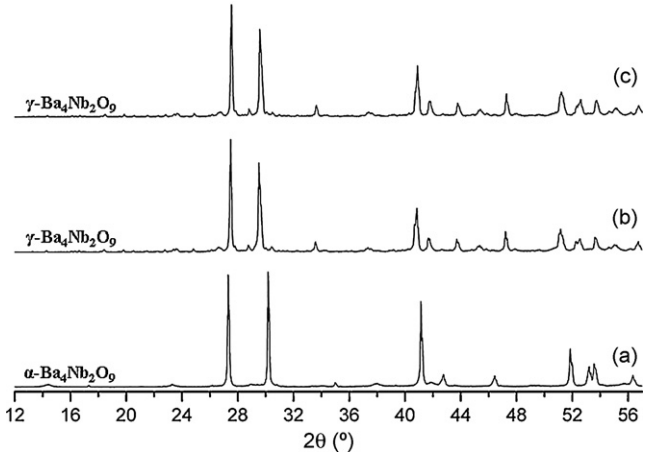

Fig. 3. X-ray diffraction patterns of $Ba_4Nb_2O_9$ samples quenched to room temperature from: (a) 1100 °C, (b) 1200 °C and (c) 1300 °C.

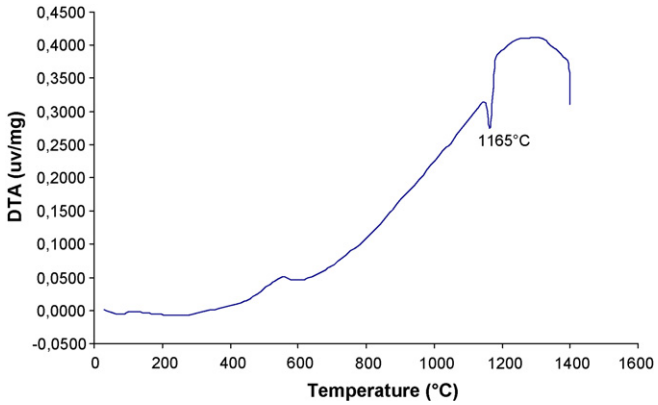

Fig. 4. A differential thermal analysis curve of the sample with the α-phase composition. The analysis was conducted at 1400 °C/5 h at a rate of 5 °C min^{-1} in an Ar atmosphere.

addition to this modification the XRD and SEM analyses of the samples quenched from $T > 1200$ °C did not reveal the presence of any other phase, which implies that the γ-modification is the high-temperature polymorph of $Ba_4Nb_2O_9$.

To determine the α → γ transition temperature, differential thermal analysis was applied. This analysis showed a sharp endothermic peak at 1165 °C during heating (Fig. 4) which could be ascribed to this phase transition. The determined transition temperature is fairly close to that reported by Leshchenko et al. (∼1130 °C).[32]

3.3. β-$Ba_4Nb_2O_9$ modification

Leshchenko et al.[32] reported that the γ-modification transforms to yet another polymorph, the β-modification, as it is heated in the range 257–317 °C. In order to prove the existence of this modification at low temperatures we annealed a pre-sintered γ-$Ba_4Nb_2O_9$ phase at 300 °C in air for 5 h. All the major peaks in the XRD spectrum of this specimen correspond to the β-$Ba_4Nb_2O_9$ phase, as described by Leshchenko (Fig. 5). Additionally, some minor reflections, which can be ascribed to $BaCO_3$, are also present in the spectrum. They could either be a consequence of the slightly more Nb_2O_5-rich chemical composition of the β-$Ba_4Nb_2O_9$ modification or it could be due to a partial decomposition of the β-$Ba_4Nb_2O_9$. Furthermore, we found that after repeated heating at 1300 °C and slow cooling

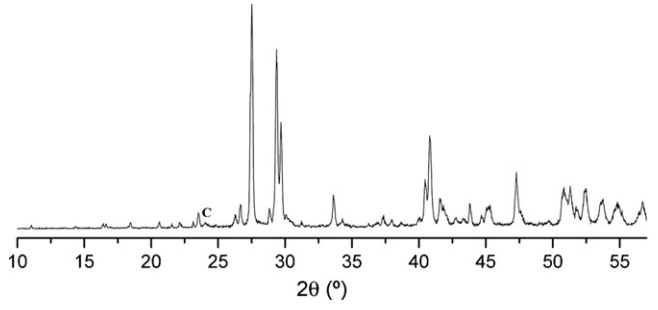

Fig. 5. X-ray powder diffraction pattern of $Ba_4Nb_2O_9$ heated at 300 °C for 5 h and quenched. Most of the diffraction peaks correspond to the β-$Ba_4Nb_2O_9$ modification (β), and C indicates minor $BaCO_3$ peaks.

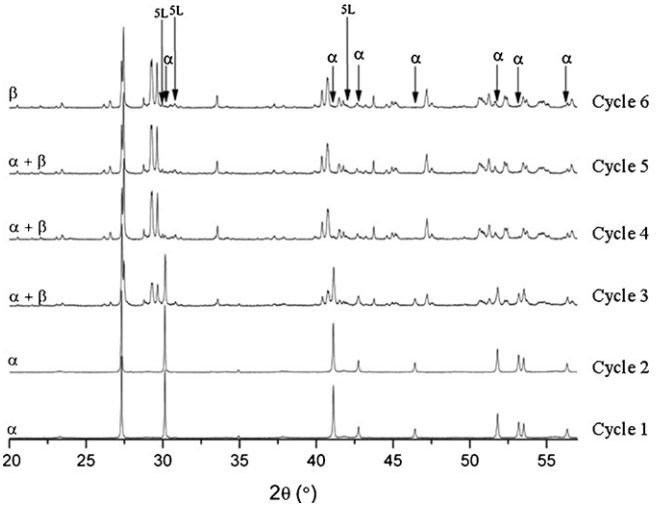

Fig. 6. X-ray diffraction patterns of $Ba_4Nb_2O_9$ show α → β phase transition. The peaks indicated by α belong to α-$Ba_4Nb_2O_9$, by β to β-$Ba_4Nb_2O_9$ and by 5L to the $Ba_5Nb_4O_{15}$.

(via an intermediate α-modification) to room temperature the $Ba_4Nb_2O_9$ progressively converts into the β-polymorph (Fig. 6). Following each firing/cooling cycle (5 h annealing time each) the samples were homogenized and re-pressed into pellets. After the third cycle some peaks of the β-$Ba_4Nb_2O_9$ modification appeared in the XRD pattern. In addition to the β- and α-peaks some low-intensity peaks that correspond to $Ba_5Nb_4O_{15}$ and $BaCO_3$ could be detected after the third cycle. The intensity of the β-peaks gradually increased with the increasing number of sintering cycles, whereas the diffraction peaks of the α-modification gradually decreased and finally disappeared in the 6th cycle (after a total of 30 h of annealing). This implies that the α-modification is a thermodynamically stable in the temperature range between 560 and 1160 °C, whereas the β-modification is stable below 560 °C.

In addition to the β-$Ba_4Nb_2O_9$, Leshchenko et al.[32] reported the existence of the β′-$Ba_4Nb_2O_9$. According to their findings, the β-phase should be converted into the hexagonal β′-modification between 530 and 700 °C. To verify the β → β′ conversion the samples of β-$Ba_4Nb_2O_9$ were fired at 590 °C. Even after longer annealing times we did not observe the formation of β′-modification in any of the samples; instead we regularly observed the presence α-$Ba_4Nb_2O_9$ in addition to $Ba_5Nb_4O_{15}$ and $BaCO_3$ peaks with significant γ-$Ba_4Nb_2O_9$ reflections after shorter annealing times. To further confirm the existence of β′-$Ba_4Nb_2O_9$ both α- and γ-$Ba_4Nb_2O_9$ samples were annealed at 560 °C for 100 h and quenched to room temperature. The composition of the samples corresponded to the α-modification, which, according to Leshchenko et al.,[32] should appear above 700 °C, whereas the expected β′-modification did not appear in the XRD spectra. In addition to α-$Ba_4Nb_2O_9$ we also observed minor $Ba_5Nb_4O_{15}$ and $BaCO_3$ reflections. The additional peaks in the X-ray spectrum that correspond to the secondary $Ba_5Nb_4O_{15}$ and $BaCO_3$ phases coincide with the peaks reported for the β′-phase, suggesting that this intermediate phase does not exist.

Although we could not confirm the existence of β′-modification of $Ba_4Nb_2O_9$ as reported by Leshchenko et al.,[32] we got a better insight into the nature of β-$Ba_4Nb_2O_9$ modification. Namely, the appearance of the γ-modification at these temperatures, the conversion of the γ-phase after quenching into the β-phase or its slow formation from α-phase after repeated reheating and grinding implies that β-modification is in fact a disordered γ-modification, i.e., γ′-$Ba_4Nb_2O_9$, where the structural changes are induced by mechanical deformation.

3.4. Stability and decomposition of the $Ba_4Nb_2O_9$ phases

Based on these results we identified the β-polymorph as the low-temperature modification observed below 500 °C, the α-polymorph as the medium-temperature modification observed in the temperature range between 560 and 1160 °C, and the γ-polymorph as the high-temperature modification found above 1160 °C.

We further investigated the stability of the individual polymorphs by annealing the pelletized samples of the γ-$Ba_4Nb_2O_9$ polymorph at 300, 560, 1000 and 1300 °C for 100 h in air. The corresponding XRD spectra recorded from the pellets' surfaces are shown in Fig. 7.

After annealing the sample at 300 °C for 100 h and quenching it to room temperature, the recorded XRD pattern corresponds to that of the β-modification, which confirms its formation at low temperatures. The XRD pattern of the sample fired at 560 °C for 100 h, where according to Leshchenko et al.[32] the β′-modification should be stable, corresponds to $Ba_5Nb_4O_{15}$ and $BaCO_3$ instead of any $Ba_4Nb_2O_9$ polymorph. The reason for the observed instability could be the reactivity with the atmosphere, as was described by Vanerah et al.[28] to be the case with the $Ba_3Nb_2O_8$ compound. After annealing at 1000 °C for 100 h and quenching to room temperature the prevailing reflections in the XRD spectrum are those of α-$Ba_4Nb_2O_9$ and $Ba_5Nb_4O_{15}$, whereas $BaCO_3$ reflections were not observed. This condition reflects the situation observed with the TEM on the α-$Ba_4Nb_2O_9$ samples, where the secondary phases were the amorphous BaO-rich phase and the nano-crystalline $Ba_5Nb_4O_{15}$, which is after an extended annealing time, well crystallized. The final sample fired at 1300 °C showed a relatively pure γ-modification with no decomposition products. These observations imply that the α-$Ba_4Nb_2O_9$ modification is very prone to decompose into $Ba_5Nb_4O_{15}$ and the BaO-rich phase, whereas the β- and γ-modifications of $Ba_4Nb_2O_9$ are more stable and do not tend to decompose either at the firing temperature or at room temperature when exposed to air. We assume that the crystal structure of the hexagonal α-polymorph, which differs from the orthorhombic β and γ, may explain its instability in the presence of water and air.

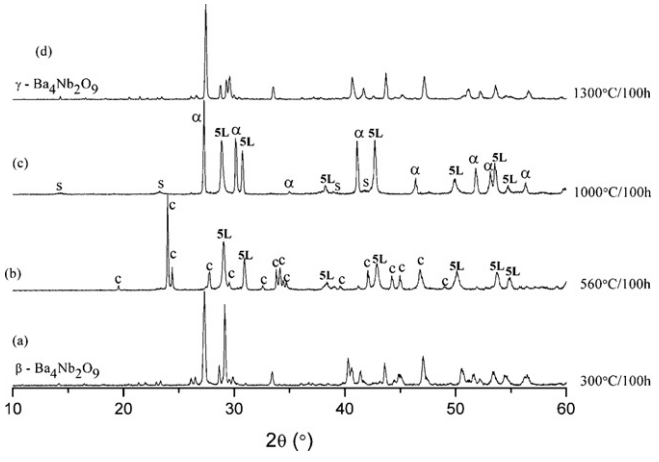

Fig. 7. X-ray diffraction pattern of the surface of pellets quenched to room temperature after annealing for 100 h at: (a) 300 °C, (b) 560 °C, (c) 1000 °C and (d) 1300 °C. The peaks indicated by α belong to α-$Ba_4Nb_2O_9$, whereas the peaks indicated by 5L and C correspond to the $Ba_5Nb_4O_{15}$ and $BaCO_3$.

4. Conclusions

The $Ba_4Nb_2O_9$ ceramic was prepared with a conventional solid-state reaction. We have isolated three $Ba_4Nb_2O_9$ polymorphs. These include the hexagonal (α) and two orthorhombic (γ, β) modifications. α-$Ba_4Nb_2O_9$ is observed in the temperature range between 560 and 1160 °C, while orthorhombic γ-$Ba_4Nb_2O_9$ is the high-temperature modification, stable above 1160 °C. The presence of low-intensity broad peaks in the X-ray spectra of the α-modification was related to remnant intergranular amorphous $BaCO_3$ and nano-crystalline $Ba_5Nb_4O_{15}$, while some of these peaks were shown to belong to superstructure reflections of α-$Ba_4Nb_2O_9$. The abundant presence of $Ba_5Nb_4O_{15}$ and $BaCO_3$ at the surfaces of sintered pellets implies that the α-modification is the least stable phase with respect to atmospheric conditions. The β-$Ba_4Nb_2O_9$ appears to be a low temperature modification of γ-$Ba_4Nb_2O_9$, i.e., γ′-$Ba_4Nb_2O_9$, observed below 560 °C, while β′-$Ba_4Nb_2O_9$ modification could not be produced at any synthesis conditions within the reported temperature ranges.

Acknowledgements

This work is based in part on the Ph.D. thesis of Jana Bezjak under Grant No. 3311-04-831835. The financial support by the Slovenian Research Agency under the Programme No. P2-0091-0106-032 entitled 'Advanced inorganic materials and technologies' is gratefully acknowledged.

References

1. Sreemoolanadhan, H., Sebastian, M. T. and Mohanan, P., High permittivity and low loss ceramics in the BaO–SrO–Nb_2O_5 system. *Mater Res Bull*, 1995, **30**(6), 653–658.
2. Vineis, C., Davies, P. K., Negas, T. and Bell, S., Microwave dielectric properties of hexagonal perovskites. *Mater Res Bull*, 1996, **31**(5), 431–437.
3. Ratheesh, R., Sreemoolanadhan, H. and Sebastian, M. T., Vibrational analysis of $Ba_{5-x}Sr_xNb_4O_{15}$ microwave dielectric ceramic resonators. *J Solid State Chem*, 1997, **131**, 2–8.
4. Kamba, S., Petzelt, J., Buixaderas, E., Haubrich, D., Vanek, P., Kuzel, P. *et al.*, High frequency dielectric properties of $A_5B_4O_{15}$ microwave ceramics. *J Appl Phys*, 2001, **89**(7), 3900–3906.
5. Moussa, S. M., Claridge, J. B., Rosseinsky, M. J., Clarke, S., Ibberson, R. M., Price, T. *et al.*, $Ba_8ZnTa_6O_{24}$: a high-Q microwave dielectric from a potentially diverse homologous series. *Appl Phys Lett*, 2003, **82**, 4537–4539.

6. Keith, G. M., Kirk, C. A., Sarma, K., Alford, N., Cussen, E. J., Rosseinsky, M. J. *et al.*, Synthesis, crystal structure, and characterterisation of $Ba(Ti_{1/2}Mn_{1/2})O_3$: a high permittivity 12R-type hexagonal perovskite. *Chem Mater*, 2004, **16**, 2007–2015.
7. Wada, K., Fukami, Y., Kakimoto, K. and Ohsato, H., Microwave dielectric properties of textured $BaLa_4Ti_4O_{15}$ ceramics. *Jpn J App Phys*, 2005, **44**(9B), 7094–7097.
8. Zhao, F., Yue, Z., Pei, J., Zhuang, H., Gui, Z. and Li, L., Improvement on the temperature coefficient of resonant frequency of hexagonal perovskites through intergrowth structures. *Appl Phys Lett*, 2006, **89**, 202901.
9. Mallinson, P., Claridge, J. B., Iddles, D., Price, T., Ibberson, R. M., Allix, M. *et al.*, New 10-layer hexagonal perovskites: relationship between cation and vacancy ordering and microwave dielectric loss. *Chem Mater*, 2006, **18**, 6227–6238.
10. Kan, A., Ogawa, H., Yokoi, A. and Ohsato, H., Microwave dielectric properties of perovskite-like structured $Ba_8Ta_6(Ni_{1-x}M_x)O_{24}$ (M = Co Cu and Zn) solid solutions. *Jpn J App Phys*, 2006, **45**(9B), 7494–7498.
11. Zhao, F., Zhuang, H., Yue, Z., Pei, J., Gui, Z. and Li, L., Phase relations and microwave dielectric properties of vanadium modified $Ba_5Nb_4O_{15}$ ceramics. *Mater Lett*, 2007, **61**, 3466–3468.
12. Zhao, F., Yue, Z., Pei, J., Gui, Z. and Li, L., Effects of octahedral thickness variance on the temperature coefficient frequency of the B-site deficient hexagonal perovskites. *Appl Phys Lett*, 2007, **90**, 142908.
13. Mitchell, R. H., *Perovskites, Modern and Ancient, Hexagonal Perovskites and Related Structures*. Almaz Press Inc., Ontario, Canada, 2007, pp. 318.
14. Kemmler-Sack, S., Die rhomboedrischen 12 L-Stapelvarianten $Ba_4M_2{}^{V}W\square O_{12}$ mit M^{V} = Nb, Ta. *Z Anorg Allg Chem*, 1979, **457**, 157–160.
15. Kemmler-Sack, S., $Ba_9Nb_6W\square_2O_{27}$ – die erste Perowskit-Stapelvariante vom rhomboedischen 27L-Typ. *Z Anorg Allg Chem*, 1980, **461**, 146–150.
16. Kemmler-Sack, S. and Treiber, U., Strukturbestimmung an $Ba_9Nb_6W\square_2O_{27}$ – der ersten Stapelvariante eines rhomboedrischen 27L-Typs. *Z Anorg Allg Chem*, 1980, **462**, 166–172.
17. Rother, H.-J., Kemmler-Sack, S., Treiber, U. and Cyris, W.-R., Die Struktur von $Ba_4Nb_2W\square O_{12}$ and $Ba_3LaNb_3\square O_{12}$. *Z Anorg Allg Chem*, 1980, **466**, 131–138.
18. Kemmler-Sack, S., Rhomboedrische 9L-Stapelvarianten in den Systemen $Ba_3W_{2-x}{}^{VI}M_x{}^{V}\square O_{9-x/2}\square_{x/2}$ mit M^{V} = Nb, Ta. *Z Anorg Allg Chem*, 1980, **471**, 102–108.
19. Kemmler-Sack, S., Hexagonale 5L-Stapelvarianten in den Systemen $Ba_5BaW_{3-x}{}^{VI}M_x{}^{V}<O_{15-x/2}\square_{x/2}$ mit M^{V} = Nb, Ta. *Z Anorg Allg Chem*, 1980, **471**, 109–114.
20. Kemmler-Sack, S. and Treiber, U., Die Struktur der rhomboedrischen 9L-Stapelvarianten $Ba_3W_{2-x}{}^{VI}Nb_x{}^{V}\square O_{9-x/2}\square_{x/2}$. *Z Anorg Allg Chem*, 1981, **478**, 198–204.
21. Bieringer, M., Moussa, S. M., Noailles, L. D., Burrows, A., Kiely, Ch., Rosseinsky, J. *et al.*, Domain growth, and zinc loss in the microwave dielectric oxide $Ba_3ZnTa_2O_{9-\delta}$. *Chem Mater*, 2003, **15**, 586–597.
22. Vanderah, T. A., Talking ceramics. *Science*, 2002, **298**, 1182–1184.
23. Galasso, F. and Katz, L., Preparation and structure of $Ba_5Ta_4O_{15}$ and related compounds. *Acta Cryst*, 1961, **14**, 647–650.
24. Shannon, J. and Katz, L., A refinement of the structure of barium tantalum oxide, $Ba_5Ta_4O_{15}$. *Acta Crystallogr B*, 1970, **B26**, 103–105.
25. Trolliard, G., Teneze, N., Boullay, Ph. and Mercurio, D., TEM study of cation-deficient-perovskite related $A_nB_{n1}O_{3n}$ compounds: the twin-shift option. *J Solid State Chem*, 2004, **177**, 1188–1196.
26. Roth, R. S. and Waring, J. L., System $BaO–Nb_2O_5$. *J Res Natl Bur Stand, Sect A*, 1961, **65**(4), 337–344.
27. Trunov, V. K., Velikodnyi, Yu. A. and Makarevich, L. G., The $BaO–Nb_2O_5$ system. *J Inorg Chem (Engl Transl)*, 1979, **24**(5), 737–739.
28. Spitsyn, V. I., Ippolitova, E. A., Kovba, L. M., Lykova, L. N. and Leshchenko, P. P., New data on the composition and polymorphism of alkaline earth metal niobates and tantalates. *Russ J Inorg Chem*, 1982, **27**(4), 464–467.
29. Leshchenko, P. P., Lykova, L. N., Kovba, L. M., Ippolitova, E. A., Shevchenko, A. V. and Lopato, L. M., The $BaO–Nb_2O_5$ system. *Izv Akad Nauk SSSR, Neorg Mater*, 1983, **19**(4), 644–647.
30. Vanderah, T. A., Collins, T. R., Wong-Ng, W., Roth, R. S. and Farber, L., Phase equilibria and crystal chemistry in the $BaO–Al_2O_3–Nb_2O_3$ and $BaO–Nb_2O_5$ systems. *J Alloys Compd*, 2002, **346**(1–2), 116–128.
31. Leshchenko, P. P., Paramova, M. V., Lykova, L. N. and Kovba, L. M., Polymorphism of the barium niobate $Ba_4Nb_2O_9$. *Vestn Mosk Univ, Khim*, 1979, **34**(2), 148–151.
32. Leshchenko, P. P., Lykova, L. N., Kovba, L. M., Stefanovich, S. Yu. and Checkin, V. V., Phase transitions in $Ba_4Nb_2O_9$. *Izv Akad Nauk SSSR, Neorg Mater*, 1985, **21**(2), 278–281.
33. Blasse, G., The new compounds with perovskite-like structures. *J Inorg Nucl Chem*, 1965, **27**, 993–1003.
34. Kemmler-Sack, S., Über hexagonale Perowskite mit Kationenfehlstellen. $Ba_{12}Ba_{22/3}M^{V}{}_{71/3}\square_2O_{33}\square_3$ (M^{V} = Nb, Ta) – die ersten Stapelvarianten eines rhomboedrischen 36L-Typs. *Z Anorg Allgem Chem (in German)*, 1981, **476**, 109–114.
35. Paramova, M. V., Leshchenko, P. P., Lykova, L. N. and Kovba, M., The polymorphism of barium tantalate $Ba_4Ta_2O_9$. *Vestn Mosk Univ, Khimiya*, 1976, **31**(4), 499–500.